Aust. J. Phys., 1990, **43**, 27–43

A Monte Carlo Investigation of $E \times B$ Discharges in Molecular Nitrogen

Michael J. Brennan,[A] *Andrew M. Garvie*[B] *and Lesley J. Kelly*

Institute for Atomic Studies, Flinders University of South Australia, Bedford Park, S.A. 5042, Australia.
[A] Present address: Atomic and Molecular Physics Laboratories, Research School of Physical Sciences, Australian National University, G.P.O. Box 4, Canberra, A.C.T. 2601, Australia.
[B] Present address: Weber Research Institute, Polytechnic University, Route 110, Farmingdale, NY 11735, U.S.A.

Abstract

A Monte Carlo simulation method has been developed and tested using the ramp model gas proposed by Reid (1979). This method is particularly useful for investigations in gases which must be modelled using many cross sections. This paper reports various phenomena associated with Townsend discharges in $\boldsymbol{E \times B}$ fields in nitrogen. Of particular interest is the relative importance of terms in the density gradient expansion of the electron energy distribution function. Simulations are conducted to assist in the interpretation of data from experimental techniques, particularly the 'photon flux' method.

1. Introduction

Solutions of the Boltzmann equation, or the use of Monte Carlo simulation techniques, in conjunction with discharge experiments, are well established procedures for verification or determination of collision cross-section data at low *E/N* (Crompton 1983). At elevated *E/N* the collision cross-section set deduced by these methods may not be unique. This is due to the relatively large number of collision cross sections required to model a gas, compared with the relatively small amount of information to be gained from conventional discharge experiments. The cross sections may be defined more stringently by measuring additional characteristics of the discharge, such as excitation rates (see e.g. Phelps and Pitchford 1985; Tachibana and Phelps 1985). Clearly, the cross sections deduced by comparisons between experiment and simulation should be independent of discharge conditions (e.g. *E/N*). The superposition of a magnetic field perpendicular to the electric field provides an additional test for the cross sections. In addition, this configuration is of interest for practical applications such as high current switches, cold cathode rectifiers and for plasma preparation.

Experiments in $\boldsymbol{E \times B}$ fields are being conducted in these laboratories using the 'photon flux' technique (Blevin 1985). Since these experiments are also capable of yielding information about electrode boundary regions (Blevin *et al.* 1985; Kelly *et al.* 1989), the Monte Carlo method was chosen for the theoretical study to augment our understanding of experimental details. This paper

0004-9506/90/010027$03.00

describes some features of the simulation technique, developed to optimise the simulation of a 'many process' gas model, and examines the influence of gradients in the electron concentration on phenomena associated with $\boldsymbol{E}\times\boldsymbol{B}$ discharges.

2. Simulation Method

The method used in the simulation is based on a 'null collision' Monte Carlo method (see e.g. Skullerud 1968; Braglia 1985). The algorithm for determining the type of event which occurs at each collision includes a technique which does not appear to have been reported in the literature.

In accordance with the null collision method, an electron is assigned initial phase space coordinates at the cathode and a mean collision time is determined from the total collision cross section:

$$Q_{\mathrm{MFT}}(\epsilon) = Q_{\mathrm{null}}(\epsilon) + \sum_{m} Q^{m}_{\mathrm{real}}(\epsilon),$$

where $Q^{m}_{\mathrm{real}}(\epsilon)$ are all the real processes considered in the model of the gas, and $Q_{\mathrm{null}}(\epsilon)$ is chosen so that

$$Q_{\mathrm{MFT}}(\epsilon) = K\epsilon^{-\frac{1}{2}},$$

where K is constant. The electron orbit is calculated between collisions and the phase space information is recorded at regular intervals of the order of a mean free time,

$$T_{\mathrm{MFT}} = (NQ_{\mathrm{MFT}}|v|)^{-1},$$

and after collisions of special interest, for external analysis. This is done by dividing phase space into a number of intervals. The resolution of these 'boxes' may be varied as required.

In 'conventional' Monte Carlo programs the possible collision probabilities are calculated at each collision by evaluating several functions defining the cross sections at the current electron energy, or by interpolating between values in a table of cross sections. Both of these methods absorb a great deal of processor time, especially where a relatively large number of possible processes are considered. This process can be accelerated by approximating the collision probabilities for any process as a set of step functions, defined on a fine set of energy 'boxes', in programs run externally to the simulation. The pre-calculated collision probabilities (PCCP, see next section for definition) for each process may be then read into the simulation program initially, as an array. There are two important limitations on the applicability of this method. First, in order to differentiate between processes in the simulation, the random numbers used in the collision routines must be of sufficient precision to assign accurate probabilities to processes with small cross sections, in a large total collision cross section. Secondly, an appropriate set of energy 'boxes', on which the probabilities are defined, must be chosen. The energy intervals may vary in size over the domain of electron energies, but must be sufficiently narrow to provide a good description of any structure in the cross sections.

In this work the magnitude of a cross section in each interval was made equal to the value at the midpoint of the interval. This in turn was determined by cubic-spline interpolation of cross-section data. A sufficient test on the appropriateness of a set of energy intervals is that they must be at least narrow enough so that the output from the simulations, principally the moments of the electron distribution and the excitation rates, is independent of box size.

The advantage of the PCCP technique is obvious: At a collision, the electron energy is related to a specific column in the probability array. A random number is sequentially tested against rows of this column to determine the collision type. Clearly, there is a significant difference between the processor time required to interrogate memory for elements of an array and that required to evaluate functions or interpolate between measured cross-section points, as is conventional practice.

Table 1. Comparison of simulation techniques for electron transport coefficients for the Reid ramp model gas: A, Penetrante *et al.* (1985); B, present work using pre-calculated collision probabilities

The uncertainty in the derived values is quoted in parentheses

$\langle\epsilon\rangle$ (eV)	W (10^6 cm s^{-1})	ND_T (10^{22} cm^{-1} s^{-1})	ND_L (10^{22} cm^{-1} s^{-1})
		$E/N = 12$ Td	
A 0·269	6·84	1·134	0·58
B 0·269 (0·001)	6·86 (0·01)	1·135 (0·002)	0·581 (0·001)
		$E/N = 24$ Td	
A 0·408	8·89	1·132	0·46
B 0·407 (0·001)	8·88 (0·01)	1·138 (0·001)	0·46 (0·01)

3. Reid Ramp Model

In order to test the PCCP technique the model gas proposed by Reid (1979) was used as a test case, since this model has been studied extensively (see e.g. Penetrante *et al.* 1985; Braglia *et al.* 1982). The properties of the model are:

Molecular weight	$M = 4 \cdot 0$ a.m.u.	
Elastic cross section	$\sigma_e(\epsilon) = 6 \cdot 0 \times 10^{-16}$ cm^2	$\epsilon > 0$ eV
Inelastic cross section	$\sigma_i(\epsilon) = 0 \cdot 0$ cm^2	$\epsilon < 0 \cdot 2$ eV
	$= 10 \times 10^{-16}(\epsilon - 0 \cdot 2)$ cm^2	$\epsilon \geq 0 \cdot 2$ eV
Gas temperature	$T = 0 \cdot 0$ K	
Gas number density	$N = 10^{17}$ cm^{-3}	

As described in the previous section an array (2 by n, where n is the number of energy boxes) was constructed on an energy grid between 0 and ϵ_{max}, where ϵ_{max} is sufficiently large so that an insignificant number of simulated electrons

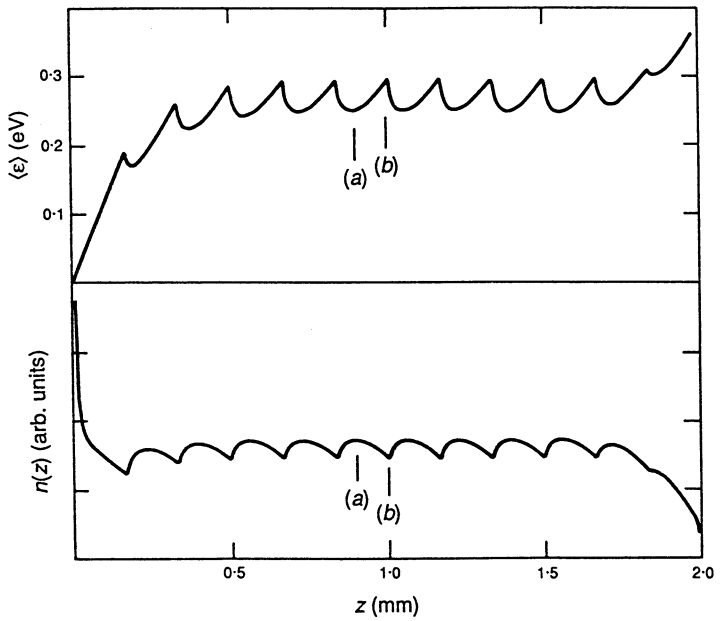

Fig. 1. Steady stream simulation of the Reid ramp model gas at 12 Td ($1\ \text{Td} \equiv 10^{-17}\ \text{V cm}^2$) showing persistent variations in the mean energy $\langle\epsilon\rangle$ and the electron number density $n(z)$. The spatial periodicity corresponds to a change in potential of 0·2 eV, the threshold of the inelastic event.

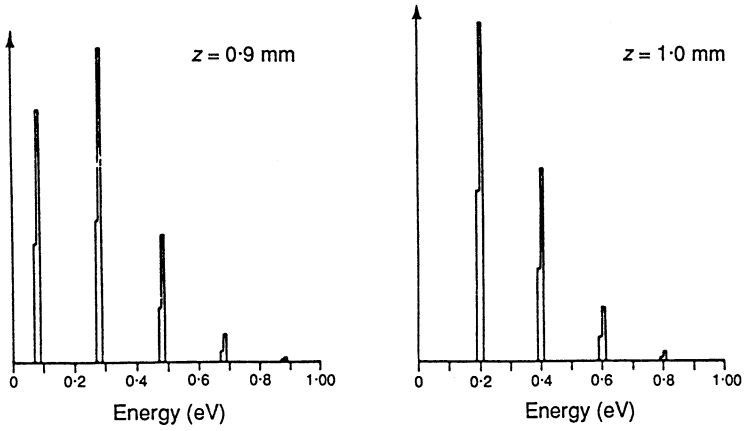

Fig. 2. Energy distribution functions for $z = 0 \cdot 9$ mm [marker (*a*) in Fig. 1] and at $z = 1 \cdot 0$ mm [marker (*b*) in Fig. 1] for the Reid model gas at 12 Td. Note that the local mean energy is smaller than the average at (*a*) and significantly higher at (*b*). This is reflected in the distribution functions at (*a*) and (*b*).

reach it. The first row of the PCCP array contains the probability of a null collision in every interval. The next row tables the probabilities for either a null event or an elastic collision. The remaining probability defines the relative likelihood of an inelastic event. Sequential comparison of a random number

with these rows determines the type of collision. Note that it is desirable to have the most probable events for mean energy electrons in the first few rows so that the testing of the array elements against the random number at collision is optimised for speed, especially in a model with many cross sections. Transport parameters for the Reid ramp model gas are compared with the work reported by Penetrante *et al.* (1985) at 12 and 24 Td in Table 1 and are found to be in excellent agreement with previous studies, lending weight to the validity of the technique.

An important feature of this model, not discussed in the literature, relates to its qualitative similarity to rare gases which generate the Holst–Oosterhuis effect (1923) (the occurrence of well separated luminous layers near the cathode in rare gas discharges). Just as is found in rare gas simulations (Hayashi 1982; Sakai *et al.* 1979; Amies *et al.* 1985), the present simulations of the Reid model yield persistent spatial variations in both the number density and the local electron energy. This is most clearly illustrated in Fig. 1, a 'steady stream' simulation. The variations in $\langle\epsilon\rangle$ and the number density, with a spatial periodicity corresponding to a potential difference of 0·2 eV, are accompanied by variations in the electron energy distribution function, which is shown for two axial positions in Fig. 2.

Interestingly however, the time dependence of the spatial moments of an isolated electron swarm in this region can be well described by the swarm averaged distribution function, as indicated by the close agreement with the calculations of Table 1. Nevertheless, there is internal structure in the swarm which is not described by the usual concentration gradient expansion. This structure persists for times much longer than the time taken for the swarm averaged drift and diffusion coefficients to become constant. This behaviour has been observed both experimentally (see e.g. Kelly *et al.* 1989; Fletcher 1985) and in many simulations (Hayashi 1982; Marode and Boeuf 1983; Amies *et al.* 1985), so that care must be taken in defining 'equilibrium', or steady state conditions.

4. Density Gradient Expansion for $E \times B$ Discharges

The macroscopic transport parameters such as drift velocity, diffusion, ionisation and excitation rates are related to the collision cross sections through the Boltzmann equation. The Boltzmann equation describes the population of elements of phase space as a function of time in terms of a probability distribution function $f(\boldsymbol{r}, \boldsymbol{v}, t)$. The distribution of electrons in velocity space may be approximated using a two term Legendre expansion:

$$f(\boldsymbol{r}, \boldsymbol{v}, t) = f_0(\boldsymbol{r}, \boldsymbol{v}, t) + (\boldsymbol{v}/v) f_1(\boldsymbol{r}, v, t) .$$

The electron concentration $n(\boldsymbol{r}, t)$ at any point in space is given by

$$n(\boldsymbol{r}, t) = 4\pi \int_0^\infty v^2 f_0(\boldsymbol{r}, v, t)\, \mathrm{d}v = \int_0^\infty f_0(\boldsymbol{r}, \epsilon, t)\, \mathrm{d}\epsilon ,$$

where $f_0(\boldsymbol{r}, \epsilon, t)$ is the symmetric term in the Legendre expansion above. For a configuration of fields that includes a magnetic field $\boldsymbol{B}_y$ lying perpendicular to

an electric field $-\boldsymbol{E}_z$, the time evolution of the symmetric part of the probability distribution function $f_0(\boldsymbol{r},\epsilon,t)$ is governed by the relation [K. Ness, personal communication (1982); cf. Holt and Haskell (1965), equations (10·84), (10·85) and (10·86) for the $B=0$ case]:

$$\frac{\partial f_0}{\partial t} - \frac{2\epsilon}{3m} M_{ij}\left(\frac{\partial^2 f_0}{\partial x_i \partial x_j} - e\frac{\partial}{\partial \epsilon}\frac{\partial (E_j f_0)}{\partial x_j}\right)$$

$$+2\epsilon^{-\frac{1}{2}}\frac{eE_i}{3m}\frac{\partial}{\partial \epsilon}\left(\epsilon^{\frac{3}{2}} M_{ij}\frac{\partial f_0}{\partial x_j} - \epsilon^{\frac{3}{2}} e M_{ij} E_j \frac{\partial f_0}{\partial \epsilon}\right) = -J_0(f_0), \qquad (1)$$

where M_{ij} are components of a tensor:

$$M_{ij} = \begin{bmatrix} \frac{\nu}{\nu^2+\omega^2} & 0 & \frac{\omega}{\nu^2+\omega^2} \\ 0 & \frac{1}{\nu} & 0 \\ -\frac{\omega}{\nu^2+\omega^2} & 0 & \frac{\nu}{\nu^2+\omega^2} \end{bmatrix}$$

In these equations ϵ is the electron energy, ν is an effective frequency of electron–molecule collisions involving momentum transfer [see Huxley and Crompton (1974) for a discussion of how inelastic collisions and isotropic scattering effect the effective momentum transfer frequency] and ω is the electron cyclotron frequency, while $J_0(f_0)$ is the rank zero Boltzmann collision integral, including elastic, inelastic and reactive collisions.

In the work reported here we are not concerned with an evaluation of terms in the Legendre expansion of $f(\boldsymbol{r},\boldsymbol{v},t)$. However, an understanding of how the symmetric term $f_0(\boldsymbol{r},\epsilon,t)$ evolves in an $\boldsymbol{E}\times\boldsymbol{B}$ discharge is required to determine the relevant transport parameters. Indeed an investigation of experimental techniques, such as the photon flux method, demands a knowledge of the effect of spatial gradients in $n(\boldsymbol{r},t)$ on excitation rates (Wedding and Kelly 1989).

To examine the influence of gradients in $n(\boldsymbol{r},t)$ on transport parameters in the $\boldsymbol{E}\times\boldsymbol{B}$ configuration, the energy distribution function is expressed in a three-dimensional gradient expansion (cf. Parker and Lowke 1969). Assuming that $f_0(\boldsymbol{r},\epsilon,t)$ can be separated into spatially dependent and energy dependent terms we have

$$f_0(\boldsymbol{r},\epsilon,t) = n(r,t)\left[g^{000}(\epsilon) - \frac{1}{\lambda_z n}\left(\frac{\partial n(r,t)}{\partial x} g^{100}(\epsilon) + \frac{\partial n(r,t)}{\partial z} g^{001}(\epsilon)\right)\right.$$

$$+\frac{1}{\lambda_z^2 n}\left(\frac{\partial^2 n}{\partial x^2} g^{200}(\epsilon) + \frac{\partial^2 n}{\partial y^2} g^{020}(\epsilon) + \frac{\partial^2 n}{\partial z^2} g^{002}(\epsilon)\right.$$

$$\left.\left.+2\frac{\partial^2 n}{\partial x \partial y} g^{110}(\epsilon) + 2\frac{\partial^2 n}{\partial x \partial z} g^{101}(\epsilon) + 2\frac{\partial^2 n}{\partial y \partial z} g^{011}(\epsilon)\right)\right] + \ldots. \qquad (2)$$

In this expansion, we have

$$\int_0^\infty g^{000}(\epsilon)\,\mathrm{d}\epsilon = 1 \quad \text{and} \quad \int_0^\infty g^{ijk}(\epsilon)\,\mathrm{d}\epsilon = 0 \ \text{ for } \ i+j+k>0,$$

where $\boldsymbol{r}$ is used to denote the coordinate system (x,y,z), and $1/\lambda_z$ $(=W_z/2D_z)$ is of the order of the characteristic length for energy exchange and is included to make $g^{ijk}(\epsilon)$ independent of pressure.

By inserting equation (2) into (1) and integrating over all electron energies one obtains, to second order in the derivatives, a continuity equation of the form

$$\begin{aligned}&\frac{\partial n}{\partial t} + \frac{\partial}{\partial x}\left(nW_{0x} - D_{Wx}\frac{\partial n}{\partial x}\right) + \frac{\partial}{\partial z}\left(nW_{0z} - D_{Wz}\frac{\partial n}{\partial z} + \ldots\right)\\ &- D_{0x}\frac{\partial^2 n}{\partial x^2} - D_{0y}\frac{\partial^2 n}{\partial y^2} - \frac{\partial^2}{\partial z^2}\left(nD_{0z} - \ldots\right) - \frac{\partial^2}{\partial x \partial z}\left(nD_{\mathrm{sh}} - \ldots\right)\\ &= n\nu_{i0} - W_{ix}\frac{\partial n}{\partial x} - W_{iz}\frac{\partial n}{\partial z} + \ldots, \qquad (3)\end{aligned}$$

where

$$W_{0x} = -\tfrac{2}{3}\frac{eE}{m}\int_0^\infty \frac{\omega}{\nu^2+\omega^2}\,\epsilon^{\frac{3}{2}}\frac{\partial}{\partial\epsilon}\left(\epsilon^{-\frac{1}{2}}g^{000}(\epsilon)\right)\mathrm{d}\epsilon,$$

$$W_{0z} = -\tfrac{2}{3}\frac{eE}{m}\int_0^\infty \frac{\nu}{\nu^2+\omega^2}\,\epsilon^{\frac{3}{2}}\frac{\partial}{\partial\epsilon}\left(\epsilon^{-\frac{1}{2}}g^{000}(\epsilon)\right)\mathrm{d}\epsilon,$$

$$W_{ix} = \frac{1}{\lambda_z}\int_0^\infty \nu_i\, g^{100}(\epsilon)\,\mathrm{d}\epsilon,$$

$$W_{iz} = \frac{1}{\lambda_z}\int_0^\infty \nu_i\, g^{001}(\epsilon)\,\mathrm{d}\epsilon.$$

The diagonal components of the apparent diffusion tensor are

$$D_{0x} = D_{0z} = \tfrac{2}{3}\frac{1}{m}\int_0^\infty \frac{\nu}{\nu^2+\omega^2}\,\epsilon g^{000}(\epsilon)\,\mathrm{d}\epsilon,$$

$$D_{0y} = \tfrac{2}{3}\frac{1}{m}\int_0^\infty \frac{1}{\nu}\,\epsilon g^{000}(\epsilon)\,\mathrm{d}\epsilon,$$

$$D_{Wx} = -\tfrac{2}{3}\frac{eE}{m}\frac{1}{\lambda_z}\int_0^\infty \frac{\omega}{\nu^2+\omega^2}\,\epsilon^{\frac{3}{2}}\frac{\partial}{\partial\epsilon}\left(\epsilon^{-\frac{1}{2}}g^{100}(\epsilon)\right)\mathrm{d}\epsilon,$$

$$D_{Wz} = -\tfrac{2}{3}\frac{eE}{m}\frac{1}{\lambda_z}\int_0^\infty \frac{\nu}{\nu^2+\omega^2}\,\epsilon^{\frac{3}{2}}\frac{\partial}{\partial\epsilon}\left(\epsilon^{-\frac{1}{2}}g^{001}(\epsilon)\right)\mathrm{d}\epsilon,$$

and the swarm averaged ionisation rate is

$$\nu_{i0} = \int_0^\infty \nu_i g^{000}(\epsilon)\, d\epsilon$$

[cf. Blevin and Fletcher (1984) for the $\boldsymbol{B} = 0$ case]. The term

$$D_{sh} = \frac{1}{3\lambda_z}\frac{eE}{m}\int_0^\infty \frac{1}{\nu^2+\omega^2}\epsilon^{\frac{3}{2}}\left[\nu\frac{\partial}{\partial\epsilon}\left(\epsilon^{-\frac{1}{2}}g^{100}(\epsilon)\right)+\omega\frac{\partial}{\partial\epsilon}\left(\epsilon^{-\frac{1}{2}}g^{001}(\epsilon)\right)\right]d\epsilon$$

is a diffusion coefficient arising from the off-diagonal terms in the diffusion tensor. This is analogous to the Hall conductivity in plasmas (see e.g. Tanenbaum 1967), and consequently we refer to it as the Hall diffusion coefficient.

Now, by collecting terms of the same order in the derivatives of the concentration, equation (3) may be rearranged and is to second order:

$$\frac{\partial n}{\partial t}+\left(W_{0x}+W_{ix}\right)\frac{\partial n}{\partial x}+\left(W_{0z}+W_{iz}\right)\frac{\partial n}{\partial z}$$

$$-\left(D_{0x}+D_{Wx}\right)\frac{\partial^2 n}{\partial x^2}-D_{0y}\frac{\partial^2 n}{\partial y^2}-D_{sh}\frac{\partial^2 n}{\partial x\partial z}-\left(D_{0z}+D_{Wz}\right)\frac{\partial^2 n}{\partial z^2}=n\nu_{i0}. \qquad (4)$$

It is clear from equation (4) how gradients in the energy distribution function can alter the 'swarm averaged' coefficients. For example, a significant degree of ionisation changes the measured axial drift velocity from W_{0z} because ionisation occurs preferentially at the front of the swarm where the mean energy is higher. It is important to realise that neither W_{ix} nor W_{iz} contribute to the electron flux, but arise from the source term in equation (1).

Experimental techniques do not resolve the components of the bracketed coefficients in equation (4), so that terms of similar dimensions in this equation may be grouped together as 'measurable' parameters:

$$\frac{\partial n}{\partial t}+W_x\frac{\partial n}{\partial x}+W_z\frac{\partial n}{\partial z}-D_x\frac{\partial^2 n}{\partial x^2}-D_y\frac{\partial^2 n}{\partial y^2}-D_z\frac{\partial^2 n}{\partial z^2}-D_{sh}\frac{\partial^2 n}{\partial x\partial z}=n\nu_{i0}. \qquad (5)$$

If the second order derivatives of equation (2) had been retained in the analysis, then third order derivatives appear in the continuity equation (5) and are related to the 'skewness' of the distribution. These second order derivatives in the gradient expansion also modify the diffusion coefficients when inserted in the source terms of equation (1). For example D_z becomes $D_{0z}+D_{Wz}+D_{iz}$, where

$$D_{iz}=\frac{1}{\lambda_z^2}\int_0^\infty \nu_i g^{002}(\epsilon)\, d\epsilon.$$

5. Production of Excited States

In an earlier paper (Blevin and Brennan 1983) an analytic solution of equation (5) was presented for a gaussian electron source and a perfectly absorbing

cathode boundary. Expressions for the electron concentration, integrated along a line of sight, were presented for steady stream and pulsed sources. These are necessary in the analysis of experimental data from the photon flux method. However, it is also necessary to relate the spatial and temporal distribution of excited states to the parent electron population, since rate coefficients for production of excited states are also affected by gradients in the electron number density. The spatially varying rate of production of states, excited by a process $Q_{(l)}$, is

$$n(\boldsymbol{r},t)\,\nu_{(l)}(\boldsymbol{r},t) = \left(\frac{2}{m}\right)^{\frac{1}{2}} N \int_0^\infty Q_{(l)}(\epsilon)\epsilon^{\frac{1}{2}} f_0(\boldsymbol{r},\epsilon,t)\,\mathrm{d}\epsilon .$$

Using the gradient expansion for $f_0(\boldsymbol{r},\epsilon,t)$ as before (cf. equation 2) we have

$$n(\boldsymbol{r},t)\,\nu_{(l)}(\boldsymbol{r},t) = n(\boldsymbol{r},t)\left(\nu_{(l)}^{000} - \nu_{(l)}^{100}\frac{1}{\lambda_z n}\frac{\partial n}{\partial x} - \nu_{(l)}^{001}\frac{1}{\lambda_z n}\frac{\partial n}{\partial z} + \ldots\right) \tag{6}$$

to first order in the gradient expansion, where

$$\nu_{(l)}^{ijk}(\boldsymbol{r},t) = \left(\frac{2}{m}\right)^{\frac{1}{2}} N \int_0^\infty Q_{(l)}(\epsilon)\epsilon^{\frac{1}{2}} g^{ijk}(\epsilon)\,\mathrm{d}\epsilon .$$

Equation (6) may be re-expressed as

$$n(x,y,z,t)\,\nu_{(l)}(x,y,z,t) = \nu_{(l)}^{000}\left(n(x,y,z,t) - \frac{\nu_{(l)}^{100}}{\nu_{(l)}^{000}}\frac{1}{\lambda_z}\frac{\partial n}{\partial x} - \frac{\nu_{(l)}^{001}}{\nu_{(l)}^{000}}\frac{1}{\lambda_z}\frac{\partial n}{\partial z} + \ldots\right). \tag{7}$$

If the gradient terms are small, then it is clear that equation (7) can be considered as an appropriate expansion of the relation

$$n(x,y,z,t)\,\nu_{(l)}(x,y,z,t) = \nu_{(l)}^{000}\, n[(x-\Delta^{100}),\, y,\, (x-\Delta^{001}),\, t], \tag{8}$$

where $\Delta^{ijk} = (1/\lambda_z)\nu^{ijk}/\nu^{000}$. That is to say, the production of excited states at any position (x,y,z) is proportional to the electron number density at $[(x-\Delta^{100}),\, y,\, (z-\Delta^{001})]$. This approximation is the key to the experimental photon flux method, when applied to $\boldsymbol{E}\times\boldsymbol{B}$ discharges.

6. Simulation Results for Discharges in Nitrogen

Some of the aspects of the behaviour of discharges mentioned above may be examined by simulation, using the PCCP technique. Molecular nitrogen was chosen as the model gas for this investigation of the phenomena associated with Townsend discharges in $\boldsymbol{E}\times\boldsymbol{B}$ fields, because it has been studied extensively in these laboratories (see e.g. Wedding *et al.* 1985). It has also been the subject of extensive theoretical study, notably by Penetrante *et al.* (1985), Phelps and Pitchford (1985), Taniguchi *et al.* (1978), Tagashira *et al.* (1980) and more recently by Ohmori *et al.* (1988).

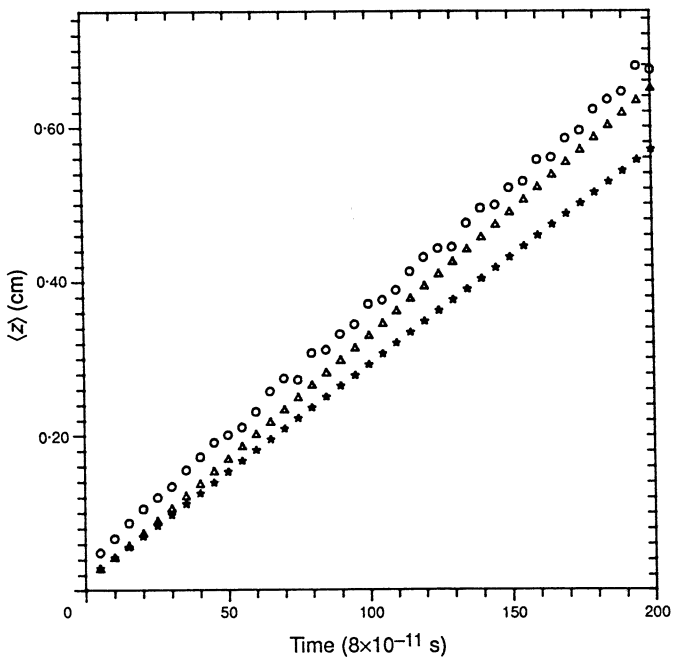

Fig. 3. Monte Carlo simulation of average position ⟨z⟩ versus time for electrons released at the cathode (○), the swarm as a whole (△), and excitation to the $C^3\Pi_u$ state (★), in an $\boldsymbol{E}\times\boldsymbol{B}$ field at $E/N = 500$ Td, $B/N = 500\times10^{-17}$ G cm^3 and $p = 1$ Torr. These yield:

○ W_z(primary electrons) = 34·67±0·01 cm μs^{-1},
△ W_z(total electrons) = 39·91±0·01 cm μs^{-1},
★ W_z(excited states) = 39·98±0·08 cm μs^{-1}.

Note that W_z(total electrons) = W_z(excited states).

In this purely theoretical study, we have adopted set C from Tagashira *et al.* (1980) and modified the set to include an excitation to the $B^2\Sigma_u^+$ state of nitrogen (Stanton and St. John 1969) and a dissociative ionisation cross section (E. E. Kunhardt, personal communication 1983). This was performed in such a way that the sum of the ionisation cross sections was identical to that by Tagashira *et al.* These alterations to the model allow comparison with the experiments of this laboratory (Kelly *et al.* 1989; Wedding and Kelly 1989), some of which have observed transitions from the $B^2\Sigma_u^+$ state.

The nitrogen model of Tagashira *et al.* is based on cross-section measurements for excitation of electronic states in nitrogen by Cartwright *et al.* (1977) and Chutjian *et al.* (1977). In order to achieve agreement between measurements of transport parameters and the calculations, Tagashira *et al.* modified the measured cross sections of Cartwright *et al.* by reducing by 15% the magnitude of the cross sections describing the excitation of electronic states with thresholds below 12·25 eV. The triplet state cross sections of Cartwright *et al.* are modelled in the present work by an exponential decay with respect to energy above 50 eV in the current work. The cross section for dissociation, as calculated using the data of Winters (1966) and Rapp *et al.* (1965), was reduced by 60%.

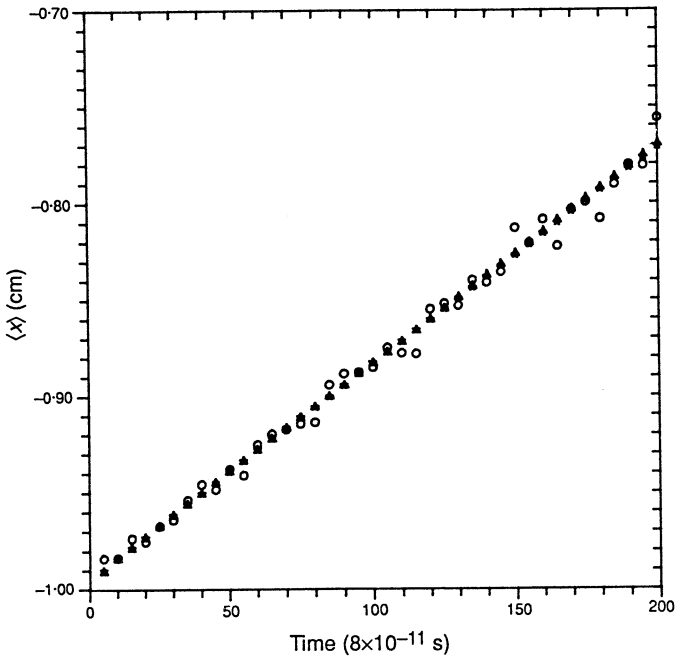

Fig. 4. Monte Carlo simulation of $\langle x \rangle$ versus time in a magnetic field at $E/N = 500$ Td, $B/N = 500 \times 10^{-17}$ G cm^3 and $p = 1$ Torr:

○ W_x(primary electrons) = 13·96±0·01 cm μs^{-1},

△ W_x(total electrons) = 14·06±0·01 cm μs^{-1},

★ W_x(excited states) = 14·15±0·08 cm μs^{-1}.

Note that W_x(primary) ≈ W_x(total) ≈ W_x(excited).

These cross sections provide a useful model of nitrogen which can be used to study the phenomena of $\boldsymbol{E \times B}$ discharges.

It should be noted that in our simulations isotropic scattering is assumed in all channels, elastic, inelastic and reactive. All electronic excitations are modelled by an excitation to the lowest vibrational level, with an energy loss equal to the threshold of that level. Following an ionising collision the residual energy was randomly partitioned between the two outgoing electrons.

Additional calculations have been performed with the data of Phelps and Pitchford (1985), allowing us to conclude that the general features discussed here are not invalidated by the particular choice of model for nitrogen, although it is expected that the detailed agreement with experimental data will be altered. Such a comparison is the subject of a future paper (Brennan and Garvie 1990).

Following the time evolution of appropriate moments of the spatial distribution of a pulsed swarm enables transport parameters to be calculated. When a magnetic field is present there are several more transport parameters to be considered, as indicated by equation (5). Figs 3 and 4 illustrate the mean position of a swarm with respect to the z and x axes, as a function of time, for $E/N = 500$ Td and $B/N = 500 \times 10^{-17}$ G cm^3 at a pressure of 1 Torr. In order to investigate the influence of density gradients on the transport parameters we have separated the evolution of the initial (primary) electrons from the group as a whole. Excitations to the $C^3\Pi_u$ state were also recorded. Several

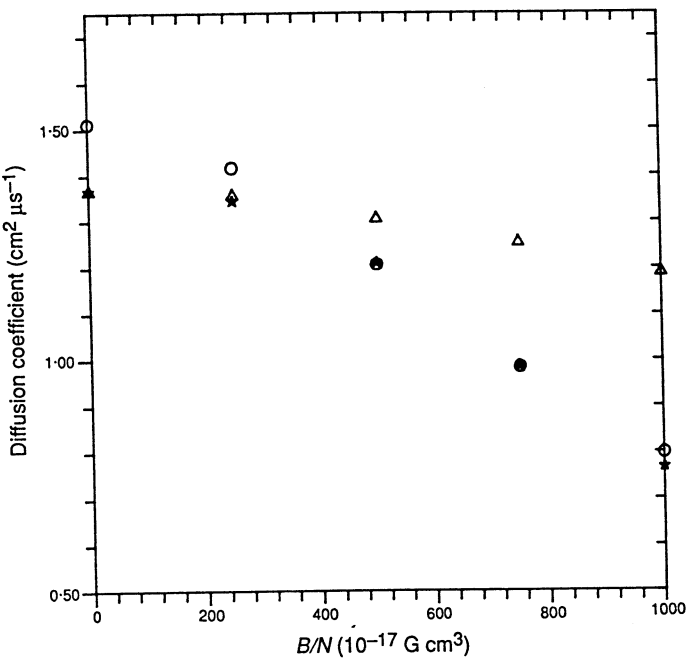

Fig. 5. Simulated values for the diagonal components of the diffusion tensor at $E/N = 500$ Td and $p = 1$ Torr for different values of magnetic field: ★, D_x; △, D_y; and ○, D_z.

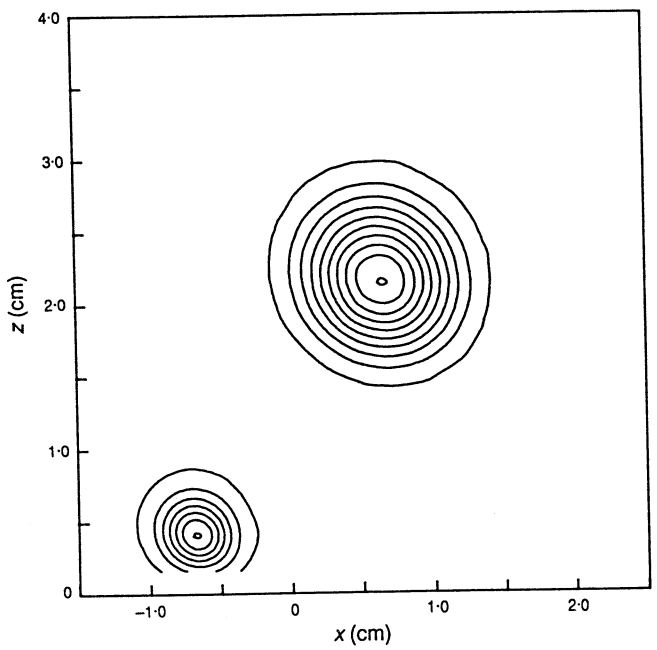

Fig. 6. Contour diagrams of electron number density, integrated along lines of sight parallel to the magnetic field at two times (see text) and for $E/N = 500$ Td, $B/N = 1000 \times 10^{-17}$ G cm^3 and $p = 1$ Torr. Contours appear at intervals of 10% of the peak height of the later swarm (16 and 80 ns).

features in these figures are worthy of comment, besides the fact that they yield values of the components of the drift velocity from the slope of the graph for the different components:

(i) Fig. 3 shows that there is a difference of approximately 13% between the z components of the drift velocity of the primary electrons and the complete swarm under these conditions. This difference is a measure of W_{iz}, since the centre of mass drift of the primary electrons is found to be equal to the instantaneously averaged velocity W_{0z}, at least within the accuracy of the simulation.

(ii) However, Fig. 4 indicates that W_{ix} is less than approximately 2% of W_{iz}!

(iii) The corresponding results for the $C^3\Pi_u$ excitations show that $\Delta^{100} \ll \Delta^{001}$ which, taken together with the previous observation, implies that $g^{100} \ll g^{001}$ for energies greater than the excitation threshold of 11·03 eV, for these conditions.

By determining the time rate of change of $\langle x^2 \rangle$, $\langle y^2 \rangle$ and $\langle z^2 \rangle$ the diagonal elements of the diffusion tensor may be found. Fig. 5 shows the dependence of the diffusion coefficients on magnetic field strength for a given E/N. The influence of the different terms in equation (4) on the 'measured' diffusion is evident. For zero magnetic field there is a clear difference between the 'longitudinal' and 'transverse' diffusion, due to the term D_{Wz} in equation (4). Note that D_x and D_y are identical within the limits of the simulation accuracy for $B = 0$, as expected. As the magnetic field is increased the mean energy of the swarm drops and produces the slow change in D_y with magnetic field. The magnetic field has a more marked effect on D_{0x} and D_{0z} (see definitions in equation 3), and these both decrease with magnetic field. At 'high' magnetic field strengths, where $\omega \approx \nu$, the situation is approached where the swarm can be roughly characterised by a diffusion along the magnetic field D_y, and across the field $D_x \approx D_z$. This implies that the terms D_{Wx} and D_{Wz} are comparable, and this is supported by other simulations (Garvie 1988) which show that $g^{100}(\epsilon)$ and $g^{001}(\epsilon)$ are comparable under these conditions.

Further characteristics of a swarm in $\boldsymbol{E} \times \boldsymbol{B}$ fields are illustrated in Fig. 6 where simulation results of the line of sight density of electrons (looking along the magnetic field) are shown for two times. The smaller swarm has only travelled 200 mean free times in our model (about 80 ps in 1 Torr of gas) and is still influenced by the cathode boundary. After 1000 mean free times the swarm has moved under the influence of the electric and magnetic fields, along the x axis and further into the drift region. Notice that in this simulation it is only after times of this order that the cathode has no further influence on the swarm development. After this time, the influence of the off-diagonal components in the diffusion tensor, which lead to the term D_{sh} (Blevin and Brennan 1983), is also evident. It causes the major axes of the contours of constant line of sight electron density, drawn at equal fractions of the peak height of the second swarm, to be rotated and changes their characteristic lengths.

Using the PCCP method it is also possible to determine the functions g^{ijk} introduced in Section 4. This is important in determining the number of terms

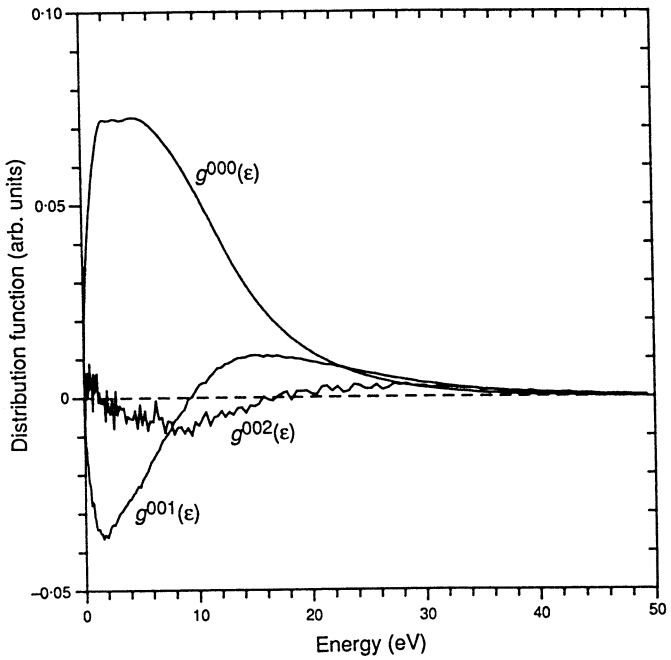

Fig. 7. Comparison between simulated determinations of $g^{000}(\epsilon)$, $g^{001}(\epsilon)$ and $g^{002}(\epsilon)$ at 500 Td for $B/N = 0$. Note that in the high energy tail $g^{000}(\epsilon)$ and $g^{001}(\epsilon)$ are of comparable size. The smaller magnitude of $g^{002}(\epsilon)$ causes difficulties in a more accurate determination.

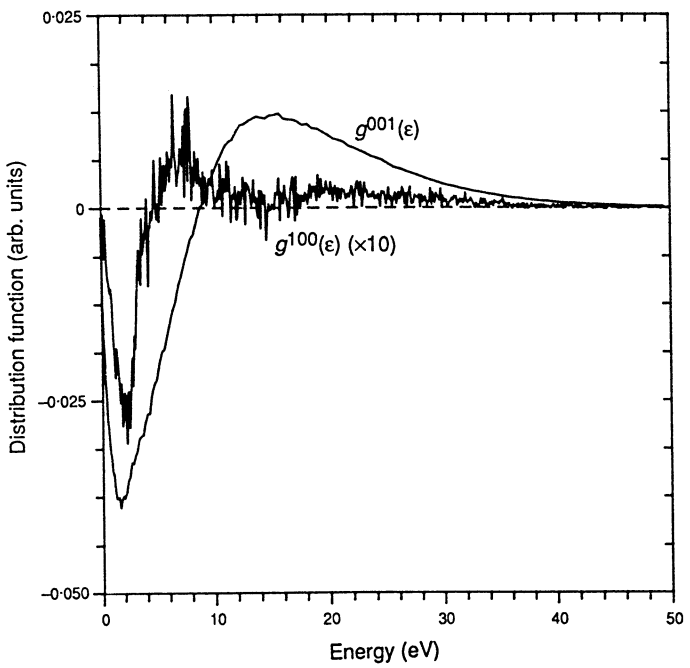

Fig. 8. Comparison between simulated determinations of $g^{100}(\epsilon)$ and $g^{001}(\epsilon)$ at $E/N = 500$ Td and $B/N = 500 \times 10^{-17}$ G cm^3.

to be included in the gradient expansion for an accurate evaluation of the transport parameters. By incorporating Kumar's (1981) method of moments into the simulation, it is possible to obtain a good estimate of the swarm averaged distribution function $g^{000}(\epsilon)$. Kumar has shown that

$$\int_x \int_y \int_z f(x,y,z,\epsilon)\,\mathrm{d}x\,\mathrm{d}y\,\mathrm{d}z = N_e\, g^{000}(\epsilon),$$

where N_e is the total number of electrons. Related expressions for the other functions $g^{ijk}(\epsilon)$ may also be derived from Kumar's work. Those of principal interest to this investigation are

$$\int_x \int_y \int_z x f(x,y,z,\epsilon)\,\mathrm{d}x\,\mathrm{d}y\,\mathrm{d}z = N_e \bar{x} g^{000}(\epsilon) + \frac{N_e}{\lambda_z} g^{100}(\epsilon),$$

$$\int_x \int_y \int_z z f(x,y,z,\epsilon)\,\mathrm{d}x\,\mathrm{d}y\,\mathrm{d}z = N_e \bar{z} g^{000}(\epsilon) + \frac{N_e}{\lambda_z} g^{001}(\epsilon),$$

$$\int_x \int_y \int_z z^2 f(x,y,z,\epsilon)\,\mathrm{d}x\,\mathrm{d}y\,\mathrm{d}z = N_e \overline{z^2} g^{000}(\epsilon) + \frac{2N_e}{\lambda_z} \bar{z} g^{001}(\epsilon) + \frac{2N_e}{\lambda_z^2} g^{002}(\epsilon).$$

The $g^{ijk}(\epsilon)$ were obtained by storing $\Sigma x(\epsilon)$, $\Sigma z(\epsilon)$ and $\Sigma z^2(\epsilon)$, together with the total number of electrons N_e over a period of 500 mean free times, at intervals of the order of a mean free time. The energy domain was represented by fine scale boxes, in a similar manner to the collision cross sections. Each electron was 'started' with the velocity components of the previously simulated electron, ensuring that the initial energy distribution corresponded to that in equilibrium. The addition of the contributions from typically 10^8 simulated collisions gives acceptably accurate representations of $g^{ijk}(\epsilon)$ for our model gas (Figs 7 and 8). Notice in Fig. 7 that the magnitudes of these functions become similar in the tail of the distribution function. This suggests that for higher energy processes there is a compelling argument that more terms may be required in the gradient expansion and hence the continuity equation (4 and 5).

The general formalism developed above makes few assumptions about the nature of the gradient expansion, save the fact that we note g^{010} must be zero and we have generally truncated our expansions at first order. However, Fig. 8 indicates that the effect of the term g^{100} on the electron energy distribution function at most energies is negligible in comparison with g^{001} for the conditions simulated, which has important implications for experiments using the photon flux technique: Remembering that the $C^3\Pi_u$ state is the usual 'probe' transition used in 'photon flux' experiments in nitrogen, it is not expected that such experiments would be sensitive to spatial gradients in x under the conditions studied, since the onset energy of the $C^3\Pi_u$ state is $11 \cdot 03$ eV, where the influence of g^{100} is trulv negligible. Under experimental conditions similar to the simulations we may simplify equation (8), considering terms involving g^{001} only. So, to a good approximation, the production of excited states at any position (x,y,z) is proportional to the electron number

density at $[x,y,(z-\Delta^{001})]$, the same approximation used for analysing discharges under the influence of an electric field only (see e.g. Wedding *et al.* 1985), although this approximation may be sensitive to the particular optical transition being studied.

7. Conclusions

A modification to the 'null collision' Monte Carlo simulation method has been developed and used to illustrate features of electron swarm behaviour in nitrogen, particularly those in $\boldsymbol{E}\times\boldsymbol{B}$ fields. Testing of the PCCP technique against the Reid ramp model gas has clearly verified previous work which suggests that under certain conditions the macroscopic behaviour of a swarm is well described by the so-called 'equilibrium transport parameters' even though the spatially resolved energy distribution function is quite distinct from its equilibrium form.

The results presented here show that the results from experiments in $\boldsymbol{E}\times\boldsymbol{B}$ fields using the photon flux technique can be successfully interpreted in terms of the swarm transport parameters, although for conditions generating high mean swarm energies an accurate analysis must include careful consideration of the effect of spatial gradients on the higher order transport coefficients.

Acknowledgments

The assistance and guidance offered by H. A. Blevin is gratefully acknowledged, as is the help of J. Mitroy and I. E. McCarthy with the design of the PCCP algorithm. This work was funded in part by the Australian Research Council and the Flinders University Research Budget. In addition we wish to acknowledge the partial financial support provided by Flinders University Research Scholarships (M.J.B. and A.M.G.), and a Commonwealth Research Scholarship and Zonta International Amelia Earhart Fellowship Award (L.J.K.).

References

Amies, B. A., Fletcher, J., and Sugawara, M. (1985). *J. Phys.* D **18**, 2023.

Blevin, H. A. (1985). XVII Int. Conf. on Phenomena in Ionised Gases, Budapest 1985 (Eds J. S. Bakos and Z. S. Uzsa Sörlei), p. 308.

Blevin, H. A., and Brennan, M. J. (1983). *Aust. J. Phys.* **36**, 859.

Blevin, H. A., and Fletcher, J. (1984). *Aust. J. Phys.* **37**, 593.

Blevin, H. A., Fletcher, J., and Hunter, S. R. (1985). *Phys. Rev.* A **31**, 2215.

Braglia, G. L. (1985). *Contrib. Plasma Phys.* **25**, 567.

Braglia, G. L., Romano, L., and Diligenti, M. (1982). *Phys. Rev.* A **26**, 3689.

Brennan, M. J., and Garvie, A. M. (1990). A study of $\boldsymbol{E}\times\boldsymbol{B}$ discharges by the photon flux method. *Aust. J. Phys.* (submitted).

Cartwright, D. C., Trajmar, S., Chutjian, A., and Winter, W. (1977). *Phys. Rev.* A **16**, 1041.

Chutjian, A., Cartwright, D. C., and Trajmar, S. (1977). *Phys. Rev.* A **16**, 1052.

Crompton, R. W. (1983). XVI Int. Conf. on Phenomena in Ionised Gases (Eds W. Bötticher *et al.*), p. 58.

Fletcher, J. (1985). *J. Phys.* D **18**, 221.

Garvie, A. M. (1988). Tomography: Application to Townsend discharges and the development of an analog technique. Ph.D. thesis. Flinders University.

Hayashi, M. (1982). *J. Phys.* D **15**, 1411.

Holst, G., and Oosterhuis, E. (1923). *Philos. Mag.* **46**, 1117.

Holt, E. H., and Haskell, R. E. (1965). 'Foundations of Plasma Dynamics' (Macmillan: New York).

Huxley, L. G. H., and Crompton, R. W. (1974). 'The Diffusion and Drift of Electrons in Gases' (Wiley–Interscience: New York).
Kelly, L. J., Brennan, M. J., and Wedding, A. B. (1989). *Aust. J. Phys.* **42**, 365.
Kumar, K. (1981). *J. Phys.* D **14**, 2199.
Marode, E., and Boeuf, J. P. (1983). XVI Int. Conf. on Phenomena in Ionised Gases (Eds W. Bötticher *et al.*), p. 206.
Ohmori, Y., Shimozuma, M., and Tagashira, H. (1988). *J. Phys.* D **21**, 724.
Parker, H. J., and Lowke, J. L. (1969). *Phys. Rev.* **181**, 302.
Penetrante, B. M., Bardsley, J. N., and Pitchford, L. C. (1985). *J. Phys.* D **18**, 1087.
Phelps, A. V., and Pitchford, L. C. (1985). *Phys. Rev.* **31**, 2932.
Rapp, D., Englander-Golden, P., and Briglia, D. D. (1965). *J. Chem. Phys.* **42**, 4081.
Reid, I. D. (1979). *Aust. J. Phys.* **32**, 231.
Sakai, Y., Tagashira, H., and Sakamoto, S. (1979). *J. Phys.* B **10**, 1035.
Skullerud, H. R. (1968). *J. Phys.* D **1**, 1567.
Stanton, P. N., and St. John, R. M. (1969). *J. Opt. Soc. Amer.* **59**, 252.
Tachibana, A., and Phelps, A. V. (1985). *J. Chem. Phys.* **71**, 3544.
Tagashira, H., Taniguchi, T., and Sakai, Y. (1980). *J. Phys.* D **13**, 235.
Tanenbaum, B. S. (1967). 'Plasma Physics' (McGraw–Hill: New York).
Taniguchi, T., Tagashira, H., and Sakai, Y. (1978). *J. Phys.* D **11**, 1757.
Wedding, A. B., Blevin, H. A., and Fletcher, J. (1985). *J. Phys.* D **18**, 2351.
Wedding, A. B., and Kelly, L. J. (1989). *Aust. J. Phys.* **42**, 101.
Winters, H. F. (1966). *J. Chem. Phys.* **44**, 1472.

Manuscript received 3 July, accepted 14 November 1989